Heterometallic Tetranuclear [Ln$^{III}_2$Co$^{III}_2$] Complexes Including Suppression of Quantum Tunneling of Magnetization in the [Dy$^{III}_2$Co$^{III}_2$] Single Molecule Magnet

Stuart K. Langley,[†] Nicholas F. Chilton,[†] Liviu Ungur,[‡] Boujemaa Moubaraki,[†] Liviu F. Chibotaru,*,[‡] and Keith S. Murray*,[†]

[†]School of Chemistry, Monash University, Building 23, Clayton, Victoria 3800, Australia

[‡]Division of Quantum and Physical Chemistry and INPAC-Institute of Nanoscale Physics and Chemistry, Katholieke Universiteit Leuven, Celestijnenlaan 200F, 3001 Heverlee, Belgium

S *Supporting Information*

ABSTRACT: Using a heterometallic approach the synthesis, structures, and magnetic properties are reported for the complexes [Ln$^{III}_2$Co$^{III}_2$(OMe)$_2$(teaH)$_2$(O$_2$CPh)$_4$(MeOH)$_4$](NO$_3$)$_2$·MeOH·H$_2$O {Ln = Gd (**1a**), Tb (**2a**), and Dy (**3a**)} and [Ln$^{III}_2$Co$^{III}_2$(OMe)$_2$(teaH)$_2$(O$_2$CPh)$_4$(MeOH)$_2$-(NO$_3$)$_2$]·MeOH·H$_2$O {Ln = Gd (**1b**), Tb (**2b**), and Dy (**3b**)}. Both compounds for the respective lanthanide ions are found to be isolated within the same crystal. Each Ln^{III} dinuclear unit is incorporated within a diamagnetic Co^{III}/organic ligand backbone utilizing triethanolamine and benzoic acid as bridging ligands. Magnetic studies reveal an absence of any observable coupling interaction for the Gd case. The Dy analogue displays single molecule magnet (SMM) behavior with a large energy barrier to magnetization reversal of 88.8 K, and the quantum tunneling of the magnetization (QTM) is effectively suppressed because of the nonmagnetic exchange ground state of the molecule. Dilution of the Dy complex into an isostructural diamagnetic yttrium matrix allowed us to determine aspects of the relaxation mechanism within the system.
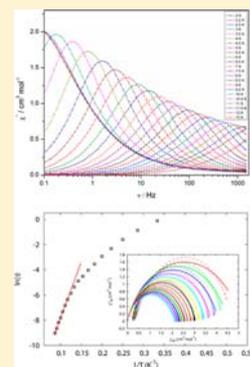
INTRODUCTION

The use of anisotropic ions of the lanthanide series such as dysprosium and terbium has led to a rapid increase in the syntheses of new and exciting compounds, many exhibiting properties of single molecule magnetism (SMM).[1] Such lanthanide-containing complexes have been shown to display SMM behavior with very large anisotropic barriers (U_{eff}) because of the intrinsic combination of orbital and spin angular momentum and strong anisotropy of these systems.[2] It has been shown that single anisotropic lanthanide ions in axial crystal field environments can display slow relaxation of the magnetization, termed single ion magnets (SIMs), with for example Ishikawa's [Pc_2Tb]$^-$ (H$_2$Pc = phthalocyanine) complex displaying an anisotropic barrier of 331 K.[3] A number of polymetallic lanthanide clusters have also been shown to display SMM behavior with large anisotropic barriers, complexes such as [Dy$_4$], [Dy$_5$], [Ho$_5$], and [Dy$_6$], displaying barriers between 170−530 K.[4] The magnitudes of these thermal relaxation barriers are much larger than what has previously been observed for polynuclear 3d clusters, where the largest was a [Mn$_6$] complex with a U_{eff} = 86 K.[5] The comparison between relaxation barriers of 4f and 3d polynuclear complexes is, however, largely unjustified as the relaxation processes are fundamentally different in each case. It appears in 4f systems, with weak exchange interactions, that the single ion anisotropy, due in large part to the crystal field effects, is the most important factor, with the exchange interaction being a secondary consideration.[6] This is in contrast to the 3d case where the exchange interactions are generally strong and total cluster anisotropy is considered. The majority of lanthanide SMMs have been isolated using Dy^{III}, as this ion has a lower tendency to exhibit quantum tunneling of the magnetization (QTM), compared to other lanthanide ions and shows very large magnetic anisotropy. We do, however, still relatively observe fast QTM in the majority of polynuclear dysprosium systems because of the hyperfine, dipolar, and exchange interactions which are problems for ideal SMM behavior. Two recent examples by Long et al., however, have been isolated and show strongly exchanged-coupled [Dy$_2$] and [Tb$_2$] complexes that are bridged via a N$_2^{3-}$ radical species resulting in U_{eff} values of 177 and 326 K and magnetic hysteresis observed at 8 and 14 K, respectively, with large coercive fields.[7] The latter compounds have the highest recorded blocking temperature for a molecular species and thus highlights the potential for lanthanide based SMMs to retain their magnetization at more practical temperatures. Such molecular based magnetic molecules potentially allow for new molecular scale devices that store or manipulate information using the orientation of their molecular spin, as well applications for use in quantum computing and molecular spintronics.[8]

Heterometallic 3d/4f complexes are also actively being researched in-order to combine the large spin of 3d ions with

the spin/anisotropy of lanthanide ions, with several SMMs so far reported.[9] We have continued our ongoing heterometallic 3d/4f triethanolamine (teaH$_3$) work[9b,10] and have isolated two dinuclear Ln^{III} species which cocrystallize within the same crystal, each encapsulated via two diamagnetic Co^{III} ions and an organic bridging shell. The complexes [Ln^{III}$_2$Co^{III}$_2$(OMe)$_2$-(teaH)$_2$(O$_2$CPh)$_4$(MeOH)$_4$](NO$_3$)$_2$·MeOH·H$_2$O {Ln = Gd (**1a**), Tb (**2a**), and Dy (**3a**)} and [Ln^{III}$_2$Co^{III}$_2$(OMe)$_2$(teaH)$_2$-(O$_2$CPh)$_4$(MeOH)$_2$(NO$_3$)$_2$]·MeOH·H$_2$O {Ln = Gd (**1b**), Tb (**2b**), and Dy (**3b**)} are thus heterometallic 3d/4f clusters, but magnetically can be considered as dinuclear Ln^{III} units. Herein we report the synthesis, structural description, magnetic properties, and ab initio theoretical description (for **3**) of the three isostructural 3d/4f cluster compounds of which two distinct molecules (**a** and **b**) are found within the asymmetric unit of each crystal structure. The results of dilution of the Dy$_2$Co$_2$ complex **3** in the diamagnetic yttrium/cobalt analogue, to elucidate relaxation mechanisms, are also described.

■ EXPERIMENTAL SECTION

General Information. All reactions were carried out under aerobic conditions. All chemicals and solvents were obtained from commercial sources and used without further purification. Elemental analyses (CHN) were carried out by Campbell Microanalytical Laboratory, University of Otago, Dunedin, New Zealand. IR spectra were recorded on a Bruker Equinox 55 spectrometer with an ATR sampler provided by Specac Inc., and the samples were run neat.

Synthesis of [Gd^{III}$_2$Co^{III}$_2$(OMe)$_2$(teaH)$_2$(O$_2$CPh)$_4$(MeOH)$_4$]-(NO$_3$)$_2$·MeOH·H$_2$O (1a) and [Gd^{III}$_2$Co^{III}$_2$(OMe)$_2$(teaH)$_2$(O$_2$CPh)$_4$-(MeOH)$_2$(NO$_3$)$_2$]·MeOH·H$_2$O (1b). Co(NO$_3$)$_2$·6H$_2$O (0.29 g, 1 mmol) and Gd(NO$_3$)$_3$·6H$_2$O (0.45 g, 1 mmol) were dissolved in MeCN (20 mL), followed by the addition of triethanolamine (0.13 mL, 1 mmol), benzoic acid (0.12 g, 1 mmol), and triethylamine (0.55 mL, 4 mmol) to give a purple solution. This was stirred for 6 h, after which the MeCN was removed and the residue redissolved in MeOH (15 mL), which was allowed to stand. Within 2−3 days blue/purple needles of **1** had crystallized, in approximate yield of 65%. Anal. Calculated (found) for **1**: Co$_2$Gd$_2$C$_{46}$H$_{70}$O$_{27}$N$_4$ (average of the two molecules in the ASU): C, 35.79 (35.60); H, 4.57 (4.32); N, 3.63 (3.64). Selected IR data ATR (cm^{-1}): 1596s, 1559s, 1491s, 1395s, 1321m, 1176w, 1091w, 1071w, 925w, 848, 820w, 721w, 688w, 609w.

Synthesis of [Tb^{III}$_2$Co^{III}$_2$(OMe)$_2$(teaH)$_2$(O$_2$CPh)$_4$(MeOH)$_4$]-(NO$_3$)$_2$·MeOH·H$_2$O (2a) and [Tb^{III}$_2$Co^{III}$_2$(OMe)$_2$(teaH)$_2$(O$_2$CPh)$_4$-(MeOH)$_2$(NO$_3$)$_2$]·MeOH·H$_2$O (2b). The same procedure was used to synthesize **2a** and **2b** except that Tb(NO$_3$)$_3$·6H$_2$O was used in place of Gd(NO$_3$)$_3$·6H$_2$O. Yield of 64%. Anal. Calculated (found) for **2**: Co$_2$Tb$_2$C$_{46}$H$_{70}$O$_{27}$N$_4$ (average of the two molecules in the ASU): C, 35.72 (35.42); H, 4.56 (4.35); N, 3.62 (3.42). Selected IR data ATR (cm^{-1}): Selected IR data ATR (cm^{-1}): 1596s, 1558s, 1491s, 1394s, 1329m, 1176w, 1092w, 1071w, 926w, 848, 821w, 721w, 688w, 612w.

Synthesis of [Dy^{III}$_2$Co^{III}$_2$(OMe)$_2$(teaH)$_2$(O$_2$CPh)$_4$(MeOH)$_4$]-(NO$_3$)$_2$·MeOH·H$_2$O (3a) and [Dy^{III}$_2$Co^{III}$_2$(OMe)$_2$(teaH)$_2$(O$_2$CPh)$_4$-(MeOH)$_2$(NO$_3$)$_2$]·MeOH·H$_2$O (3b). The same procedure was used to synthesize **3a** and **3b** except that Dy(NO$_3$)$_3$·6H$_2$O was used in place of Gd(NO$_3$)$_3$·6H$_2$O. Yield of 70%. Anal. Calculated (found) for **3**: Co$_2$Dy$_2$C$_{46}$H$_{70}$O$_{27}$N$_4$ (average of the two molecules found in the ASU): C, 35.56 (35.20); H, 4.54 (4.02); N, 3.61 (3.84). Selected IR data ATR (cm^{-1}): 3487w, 1594s, 1554s, 1483s, 1388s, 1285m, 1219w, 1176w, 1122w, 1088w, 1068w, 1022w, 944w, 921w, 846w, 812w, 742w, 716w, 687w, 641w, 610w.

X-ray Crystallography. X-ray measurements were performed at 100(2) K at the Australian synchrotron MX1 beamline. The data collection and integration were performed within Blu-Ice[11] and XDS[12] software programs. Compounds (**1a, 1b**), (**2a, 2b**), and (**3a, 3b**) were solved by direct and Patterson methods (SHELXS-97), and refined (SHELXL-97) by full least matrix least-squares on all F^2 data.[13] Crystallographic data and refinement parameters for **1**, **2**, and **3** are summarized in Table 1. Crystallographic details are available in the

Table 1. Crystallographic Data for Compounds (1a, 1b), (2a, 2b), and (3a, 3b)

	1a, 1b (1)	2a, 2b (2)	3a, 3b (3)
formula^a	Co$_2$Gd$_2$C$_{46}$H$_{70}$N$_4$O$_{27}$	Co$_2$Tb$_2$C$_{46}$H$_{70}$N$_4$O$_{27}$	Co$_2$Dy$_2$C$_{46}$H$_{70}$N$_4$O$_{27}$
M/g mol^{-1}	1543.40	1546.73	1553.90
crystal system	tetragonal	tetragonal	tetragonal
space group	$I4_1/a$	$I4_1/a$	$I4_1/a$
a/Å	41.177(3)	41.073(6)	40.986(6)
b/Å	41.177(3)	41.073(6)	40.986(6)
c/Å	16.114(3)	15.970(3)	15.985(3)
α/deg	90	90	90
β/deg	90	90	90
γ/deg	90	90	90
V/Å^3	27323(5)	26942(8)	26852(9)
T/K	100(2)	100(2)	100(2)
Z	16	16	16
ρ_{calc}/g cm^{-3}	1.499	1.521	1.535
λ^b/ Å	0.71090	0.71090	0.71070
data measured	45309	119509	174458
ind. reflns	15590	17028	11791
R_{int}	0.0583	0.0642	0.0419
reflns with $I > 2\sigma(I)$	11261	15852	11562
parameters	783	772	787
restraints	128	201	150
$R_1{}^c$(obs)	0.0578	0.0616	0.0543
$wR_2{}^c$(all)	0.1630	0.2031	0.1572
goodness of fit	1.037	1.078	1.049
largest residuals/ e Å^{-3}	3.345, −1.470	2.669, −2.097	2.962, −2.021

^{a}The average formula of the two molecules is given, including solvate molecules. ^{b}Graphite monochromator. ^{c}R$_1$ = $\sum||F_o| - |F_c||/\sum|F_o|$, wR$_2$ = $\{\sum w(F_o{}^2 - F_c{}^2)^2/\sum w(F_o{}^2)^2\}^{1/2}$.

Supporting Information in CIF format. CCDC numbers 885502 to 885504 (**1** to **3**) and 903131 (**4** (see later); Supporting Information). These data can be obtained free of charge from the Cambridge Crystallographic Data Centre via www.ccdc.cam.ac.uk/data_request/cif.

Magnetic Measurements. The magnetic susceptibility measurements were carried out on a Quantum Design SQUID magnetometer MPMS-XL 7 operating between 1.8 and 300 K for direct current (DC) applied fields ranging from 0−5 T. Microcrystalline samples were dispersed in Vaseline to avoid torquing of the crystallites. The sample mulls were contained in a calibrated gelatin capsule held at the center of a drinking straw that was fixed at the end of the sample rod. Alternating current (AC) susceptibilities were carried out under an oscillating AC field of 3 Oe and frequencies ranging from 0.1 to 1500 Hz.

■ RESULTS AND DISCUSSION

Crystal Structure Descriptions. Single crystal X-ray analysis shows that compounds **1a, 1b** (Supporting Information, Figure S1), **2a, 2b** (Supporting Information, Figure S2), and **3a, 3b** (Figure 1 and Supporting Information, Figure S3) are isostructural; therefore, the description of the Dy analogue will only be given here. Complexes **3a** and **3b** are heterometallic tetranuclear complexes which crystallize in the tetragonal space group $I4_1/a$, with the asymmetric unit consisting of one-half of both **3a** and **3b**, with one unique Dy^{III} and Co^{III} ion for each, as well as partially occupied solvent MeOH and H$_2$O molecules. Structurally **3a** and **3b** are close to being identical; **3a** is found to have two terminal MeOH
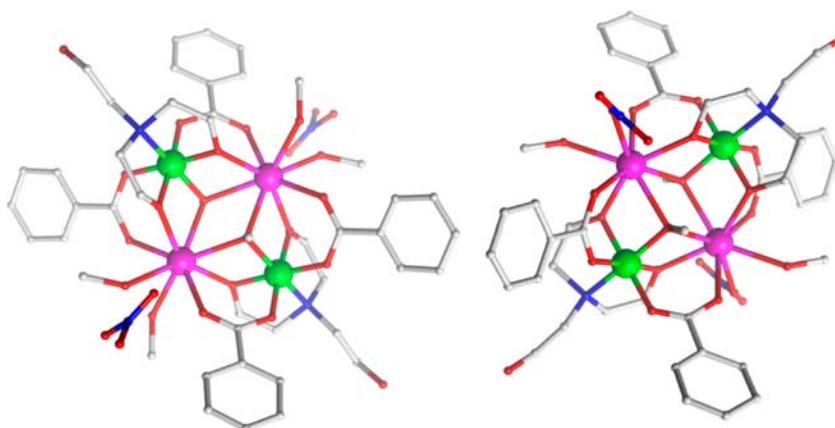
Figure 1. Structure of **3a** (left) and **3b** (right) in the crystal. Disordered and H-atoms are omitted for clarity. Color scheme: Co[III], Green; Dy[III], purple; O, red; N, blue; C, light gray.

Table 2. Selected Bond Distances (Å) for Complexes 1−3[a]

molecule a	1a (Gd)	2a (Tb)	3a (Dy)	molecule b	1b (Gd)	2b (Tb)	3b (Dy)
Ln2−O17	2.289(6)	2.258(7)	2.235(6)	Ln1−O4[II]	2.288(6)	2.254(7)	2.235(6)
Ln2−O16[I]	2.290(6)	2.292(6)	2.281(6)	Ln1−O5	2.299(6)	2.298(6)	2.270(6)
Ln2−O20	2.374(6)	2.334(7)	2.324(7)	Ln1−O8	2.358(6)	2.331(6)	2.322(7)
Ln2−O15[I]	2.367(6)	2.330(7)	2.341(6)	Ln1−O3[II]	2.379(7)	2.346(6)	2.331(7)
Ln2−O21	2.443(7)	2.474(8)	2.422(8)	Ln1−O12	2.428(7)	2.441(8)	2.412(7)
Ln2−O13[I]	2.443(6)	2.466(6)	2.428(6)	Ln1−O1[II]	2.451(5)	2.423(6)	2.435(6)
Ln2−O22	2.439(7)	2.421(7)	2.441(7)	Ln1−O1	2.483(5)	2.499(6)	2.470(6)
Ln2−O13	2.461(6)	2.439(6)	2.448(6)	Ln1−O9	2.486(6)	2.462(7)	2.480(7)
Co2−O16	1.882(6)	1.897(7)	1.890(6)	Co1−O5	1.866(6)	1.892(6)	1.876(6)
Co2−O17	1.878(6)	1.908(7)	1.891(7)	Co1−O4	1.863(6)	1.918(7)	1.896(7)
Co2−O19	1.903(6)	1.909(7)	1.896(7)	Co1−O2	1.916(6)	1.920(6)	1.905(6)
Co2−O14	1.916(6)	1.930(7)	1.924(7)	Co1−O1	1.931(6)	1.927(6)	1.927(6)
Co2−O13	1.943(5)	1.929(6)	1.929(6)	Co1−O7	1.933(6)	1.937(6)	1.952(6)
Co2−N3	1.968(7)	1.968(8)	1.964(8)	Co1−N1	1.987(7)	1.962(8)	1.964(7)

[a]Symmetry transformation: (I) − x, 1 − y, 2 − z; (II) 1/2 − x, 1/2 − y, 3/2 − z.

molecules coordinated to the Dy[III] ion, with a nitrate counterion in the lattice that is H-bonding to one of the MeOH molecules. **3b** has one coordinated MeOH, with the nitrate now coordinating to the Dy[III] site and with the second methanol now found in the lattice, H-bonding to the nitrate. Thus **3a** is cationic and **3b** is neutral. For descriptive purposes **3a** and **3b** can be considered as equivalent and subsequently both will be described as compound **3** (similarly for **1a** + **1b** ≡ **1** and **2a** + **2b** ≡ **2**). Complex **3** (Figure 1) consists of two Co[III] and two Dy[III] ions, with the metallic core best described as a planar butterfly motif, with the Dy[III] ions occupying the body positions and the Co[III] ions the outer wing-tips. The core is stabilized by two μ_3 methoxide ligands, both bridging to two Dy[III] ions and one Co[III] ion. Around the periphery of the cluster are four benzoate ligands each displaying the *syn, syn μ* bonding mode, bridging a Co[III] to a Dy[III] ion. There are also two doubly deprotonated teaH[2−] ligands, both displaying the μ_3:η^2:η^2:η^1:η^0 bonding mode, with the N-atom coordinating to a wing-tip Co[III] ion and the O-atoms bridging from the Co[III] to the body Dy[III] ions, with the protonated alcohol arm being non-coordinating. The two Co[III] ions are six coordinate with octahedral geometries with an average Co-L$_{N,O}$ bond length of 1.916 Å (**a**) and 1.920 Å (**b**). The two Dy[III] ions are eight coordinate with distorted square antiprismatic geometries with an average Dy−O bond length of 2.365 Å (**a**) and 2.371 Å (**b**). SHAPE software quantified this geometry with continuous

shape measure deviations of 0.865 (Dy ion of **3b**) and 0.924 (Dy ion of **3a**).[14] The intramolecular Dy···Dy distance is 4.075(7) (**a**) Å and 4.088(6) Å (**b**), while the Dy−O−Dy angle is 113.3(2) (**a**) and 112.9(2)° (**b**). The closest intermolecular Dy···Dy distance is 7.56 Å. Selected bond lengths for **1−3** are given in Table 2. Intermolecular H-bonds are found for **3** between the terminal MeOH and the coordinated/non-coordinated nitrate ions, forming one-dimensional (1-D) chains along the *c*-axis (Supporting Information, Figure S4). Further to this, edge-to-face aromatic C−H···π interactions occur between the benzoate ligands, the C−H groups however are not directed toward the ring centroids, with closest contacts of 2.61−3.1 Å found (Supporting Information, Figure S5). This arranges the clusters in such a way that the crystal packing reveals the presence of channels running along the *c*-axis (Figure 2). Two types of channels are present; the first contains the free, non-coordinating teaH[2−] arms, as well as disordered MeOH and H$_2$O solvent molecules, while the second channel consists of disordered MeOH solvent molecules. When the MeOH molecules are omitted it is found that the closest contact within the channel is ∼9.1 Å.

Magnetic Properties. The bulk magnetic properties of **1−3** were probed via variable temperature, DC and AC susceptibility measurements on polycrystalline samples. The DC studies (Figure 3) reveal room temperature $\chi_M T$ values of 15.71, 23.14, and 26.00 cm³ mol⁻¹ K in good agreement with
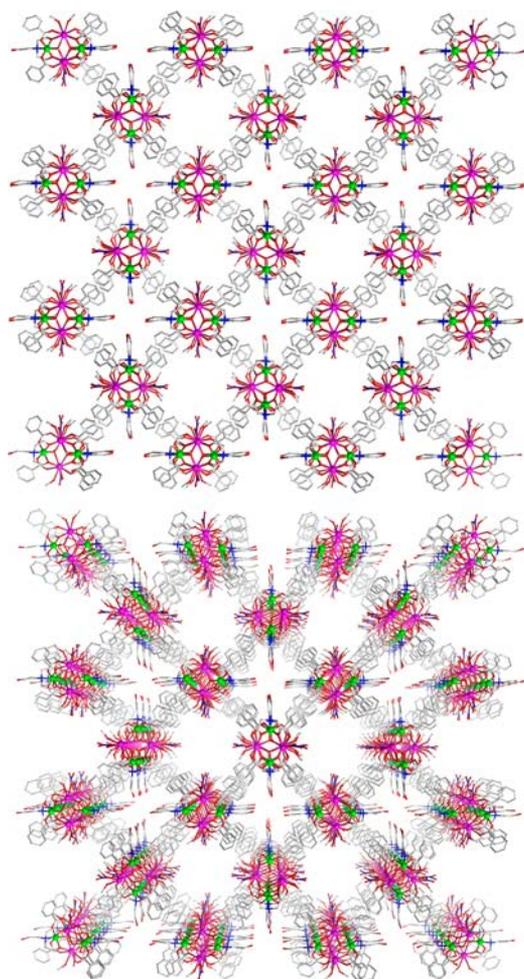
Figure 2. Packing of **3a** and **3b**; (top); a 2-D view. (Bottom); a perspective view down the *c*-axis highlighting the channels. The H atoms and solvent molecules have been removed for clarity.
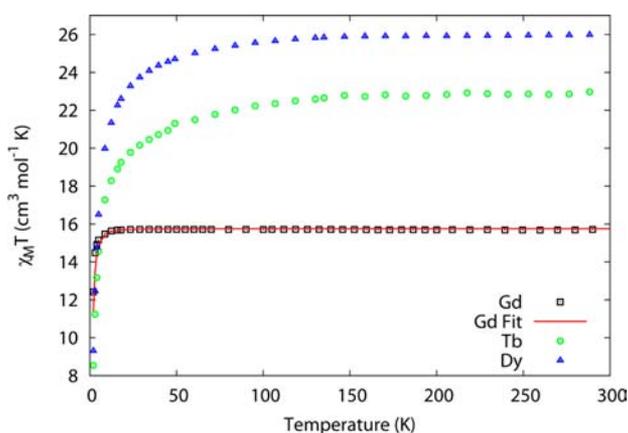

Figure 3. Plots of $\chi_M T$ vs T for **1**−**3** measured at 0.5 (**1**) and 1 T (**2** and **3**) and in the 2 to 300 K temperature range. The solid red line is a fit of the experimental data for the Gd complex **1** using the parameters given in the text.

the expected value of 15.76, 23.64, and 28.34 cm^3 mol^{-1} K for two uncoupled Gd^{III}, Tb^{III}, and Dy^{III} ions, respectively. For the isotropic case **1**, upon lowering the temperature the $\chi_M T$ product remains constant until below 10 K where a sharp decrease is observed. To investigate the interaction between the

two paramagnetic Gd^{III} ions, simultaneous fitting of the susceptibility and magnetization data was attempted by use of the program PHI^{15} using an isotropic single-*J* model corresponding to the Hamiltonian $\hat{H} = -2J\hat{S}_1 \cdot \hat{S}_2 + g\beta(\hat{S}_1 + \hat{S}_2) \cdot H$, employing a nonperturbative, field dependent method. It was determined that the magnitude of the exchange coupling interaction was smaller than experimental error as extremely accurate correspondence to the data was obtained for $J = 0$ cm^{-1} and $g = 2.00$ (Figure 3 and Supporting Information, Figure S6, red lines). Obviously this situation renders all the spin states degenerate in energy, and the drop in $\chi_M T$ at low temperatures is therefore solely due to depopulation of the Zeeman split m_S states.

As the temperature is lowered for the anisotropic cases **2** and **3**, the $\chi_M T$ values decrease very gradually (300−50 K) before a much bigger decrease occurring below 50 K, reaching a value of 10.71 and 13.47 cm^3 mol^{-1} K at 0.1 T and 2 K for **2** and **3**, respectively. The decrease in $\chi_M T$ is due to the depopulation of the m_J sublevels of the ground *J* state, with the possibility of antiferromagnetic exchange/dipolar interactions also present. The *M* vs *H* plots, shown in the Supporting Information as Figures S7 and S8, each show sharp increases with increasing *H*, at low fields and low temperatures, with *M* then increasing linearly at larger fields, reaching a value of 9.05 and 9.77 *Nβ* at 2 K and 5 T, for **2** and **3**, respectively. These values are much lower than expected for two isolated Tb^{III} and Dy^{III} ions of 18 and 20 *Nβ*, because of the crystal-field effects at the Ln^{III} ions eliminating the degeneracy of the ground *J* state.

AC susceptibility measurements in a zero DC applied field reveal features typical of SMM behavior for the Dy complex **3**. Both the in-phase (χ_M') and out-of-phase (χ_M'') susceptibilities display frequency and temperature dependence below 20 K, signaling the blocking of the magnetization due to an anisotropy barrier (Figure 4 and Supporting Information, Figure S9). A plot of χ_M'' vs *v* isotherms (Figure 4, top), reveals frequency dependent maxima down to 3 K and 0.1 Hz. From these data, Cole−Cole plots of χ_M'' vs χ_M' (Figure 4, bottom-inset) were constructed and fitted to a generalized Debye model to determine α values and relaxation times (τ) in the temperature range 4−10.5 K. The plots reveal relatively symmetrical semicircles, indicating a single relaxation process, with α values ranging from 0.29−0.24, indicating a broad distribution of relaxation times in this single relaxation process. These slightly larger α values than those reported for previous [Dy$_2$] complexes, may be due to the presence of two different Dy^{III} sites found for **3a** and **3b** and the slight changes in the ligand field caused by the replacement of the nitrate for the MeOH. From the frequency-dependent behavior, it was found that the relaxation follows a thermally activated mechanism above 8.5 K and plots of $\ln(\tau)$ vs $1/T$ are linear (Figure 4, bottom). Fitting to the Arrhenius law [$\tau = \tau_o \exp(U_{eff}/k_B T)$] afforded values of $U_{eff} = 88.8(2)$ K and $\tau_o = 5.64 \times 10^{-8}$ s (R = 0.9974). This result indicates a large barrier to thermal relaxation, with the pre-exponential factor consistent with the expected value for a SMM of between 10^{-6}−10^{-11}.^{16} Below 8.5 K the plot deviates slightly from linear behavior indicating that QTM may be becoming active. The relaxation time, τ, does not, however, become temperature independent in the temperature range studied, indicating the absence of a pure quantum regime down to 2.5 K (when the tunneling rate becomes faster than the thermally activated relaxation). The value of τ expected if the relaxation process was to crossover into a pure quantum regime, below 2.5 K, indicates that the
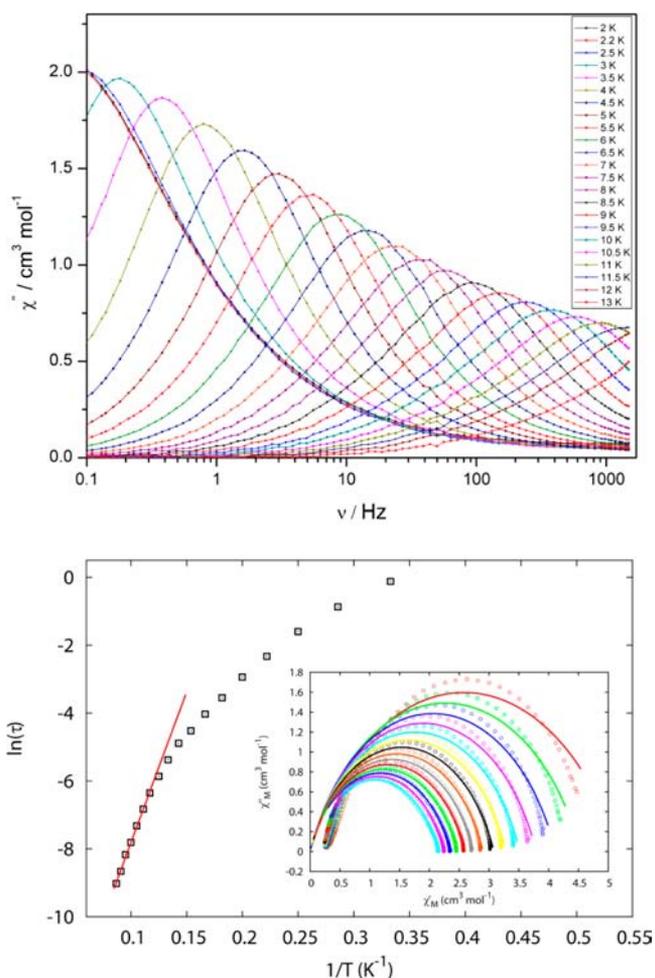
Figure 4. (top), Frequency dependence of the out-of-phase AC susceptibility, χ_M'', of **3** below 13 K, under zero applied DC field. (Bottom) Magnetization relaxation time $\ln(\tau)$ vs T^{-1} ($H_{DC} = 0$). The solid red line is a fit with the Arrhenius law (see text); inset Cole−Cole plots between 4−10.5 K, with the solid lines being best fits to the experimental data (see text).

characteristic tunneling rate would be relatively slow (>1 s) when compared to previously reported Dy^{III} SMMs (usually on the ms scale).[17] In many previously reported lanthanide SMMs, a second increase of the χ_M' and χ_M'' components at low temperatures is often observed because of QTM.[6a,b] In the case of **3**, however, the χ_M' and χ_M'' components are minimal as the temperature reaches 2 K, with no temperature independent peaks observed from the χ_M'' (T,ν) data. Upon application of a static DC field, a technique used to reduce quantum tunneling effects, no significant shift in the maximum position of the temperature in the χ_M'' vs T plot was observed in fields up to 1000 Oe (Supporting Information, Figure S10), further suggesting that QTM is inefficient in this system.

AC studies for the Tb analogue **2** revealed an absence of any out-of-phase susceptibility peaks in zero DC field (Supporting Information, Figure S11). Performing applied DC field experiments for **2** revealed frequency dependent maxima in the out-of-phase signal, indicating field induced SMM behavior. This behavior is observed only upon application of a static field and is likely due to the suppression of the quantum tunnelling of the magnetization between sublevels, which is very fast at zero field. Such activity is known for many lanthanide SMMs[18]

and is commonly observed in terbium systems because of the non-Kramers nature of the ion. This allows for the mixing directly by the crystal-field of opposing projections of the ground state angular momentum such that tunnelling pathways are often readily available. Studies were performed in fields of 1 and 1.75 T (Supporting Information, Figure S12) with anisotropic barriers found to be 14.31(1) and 18.99(1) K and with pre-exponential factors of 2.84×10^{-6} and 6.02×10^{-6} s, respectively (Supporting Information, Figure S13).

Only a limited number of examples have displayed efficient suppression of zero-field tunneling for Ln^{III} complexes. These include the radical-bridged [Dy$_2$] and [Tb$_2$] complexes that undergo strong exchange coupling[7] and a weakly ferromagnetically coupled [Dy$_2$] complex reported by Guo et al., who noted a pure quantum regime being observed below 0.15 K with a characteristic tunnelling time (τ_{QTM}) of 35 s, some 3 orders of magnitude slower than for other reported Dy^{III} complexes.[17] The behavior in the latter example[17] was attributed to the almost parallel alignment of the local anisotropy axes along the Dy−Dy vector, resulting in strong Ising-type dipolar exchange and therefore small transverse dipolar interactions leading to low QTM.

To determine the single-ion properties and the interactions between the Dy^{III} ions, ab initio calculations were performed to determine the potential reasons for the reduced QTM in compound **3**.

Ab Initio Calculations of Single-Ion and Exchange Coupling in the Dy$^{III}_2$Co$^{III}_2$ Example 3. All calculations were done with MOLCAS 7.6 and are of CASSCF/RASSI/SINGLE_ANISO type. Two structural models for the mononuclear Dy fragments have been employed: fragment **A** (small) and **B** (large). The structural model **A** for one of the molecules of **3** is shown in Figure 5. The fragment for the second unique molecule in the asymmetric unit is similar. Model **B** is the complete complex **3**, and in both cases the
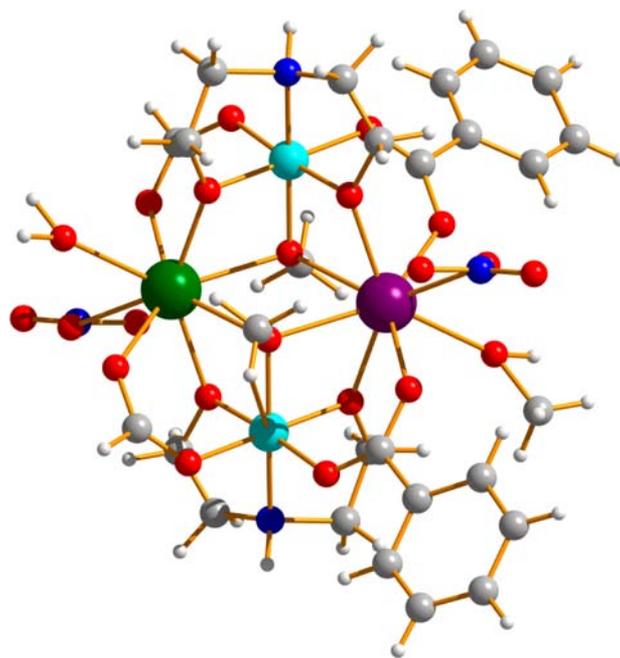

Figure 5. Structure of fragment **A** for molecule **3a**. Fragment **A** of molecule **3b** is similar. Color scheme: Dy, purple; Lu, green; O, red; N, blue; C, gray; Co, light blue.
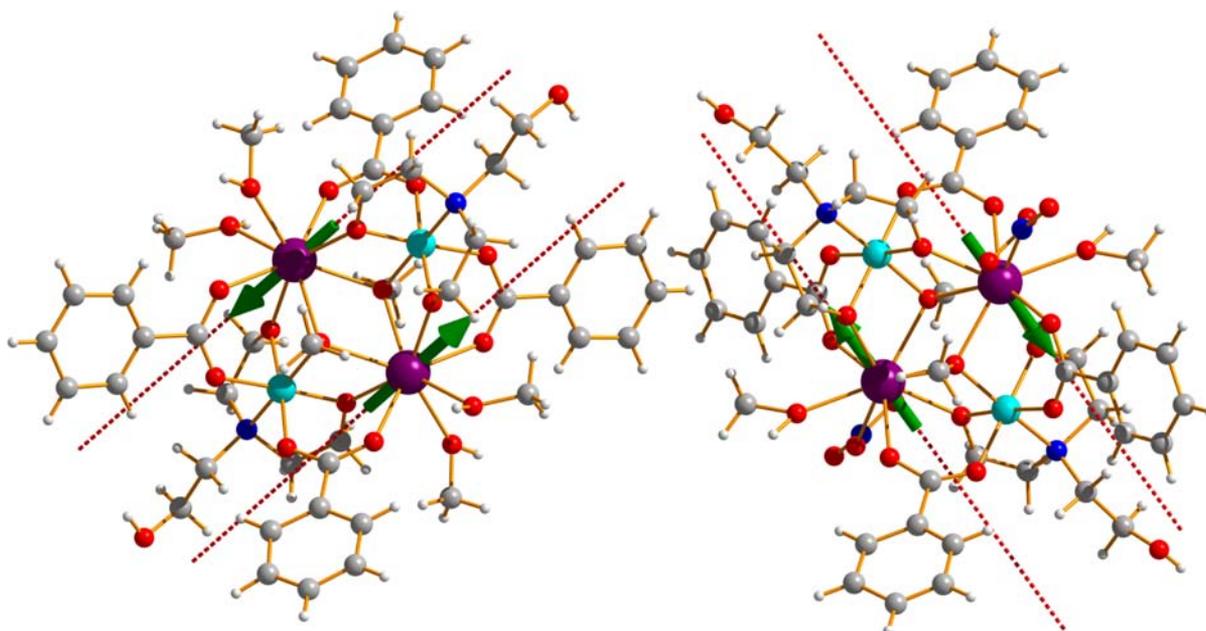
Figure 6. Orientation of the local magnetic moments in the ground doublet of **3a** (left) and **3b** (right). Green arrows show the antiferromagnetic coupling of the local magnetic moments of the Dy ions in the ground state.

neighboring Dy ion was computationally substituted by the diamagnetic Lu, the latter chosen rather than Y because it is much closer electronically to Dy. The Co ions were kept the same in all calculations.

Two basis set approximations have been employed: λ − small, and θ − large. Supporting Information, Table S1 shows the contractions of the employed basis sets for all elements. The active space of the CASSCF method included 9 electrons in 7 orbitals (4f orbitals of Dy^{3+} ion) and 21 sextets, 128 quartets, and 130 doublet states were mixed by spin−orbit coupling. On the basis of the resulting spin−orbital multiplets, the SINGLE_ANISO program was used to compute local magnetic properties (g-tensors and magnetic axes). The calculated free ion electronic and magnetic properties of the individual Dy ions on both molecules, (Supporting Information, Table S2−S5) show that the local g-tensors on the dysprosium sites are strongly axial, with values for the energies of the first excitations of the Dy sites on both individual molecules being close in energy at about 90−100 cm^{-1}. This is consistent with the observation of a single thermally activated relaxation regime in the AC data. The orientation of the main anisotropy axes of the ground Kramers doublets of the individual ions are almost parallel to each other, differing in direction by no more than 4° (Figure 6, Supporting Information, Tables S6 and S7). The angle between the roughly parallel single ion anisotropy axes of the two different molecules is calculated to be 80−83°, Supporting Information, Table S8.

The exchange interactions have been considered within each complex, employing the Ising exchange Hamiltonian, eq 1, where the anisotropic dipolar and exchange interactions are treated within the Lines model.[19]

$$H = -(J_{dip} + J_{exch})\hat{\tilde{s}}_{1,z}\hat{\tilde{s}}_{2,z} \tag{1}$$

where $\hat{\tilde{s}}_{1,z} = 1/2$ is the projection of the pseudospin corresponding to the lowest Kramers doublet of each ion onto the main anisotropy axis z. The dipolar contribution is

considered exactly, while the exchange part is determined from a fit to the magnetic data. The best fits of the magnetic properties, Figure 7 and Supporting Information, Figure S14, are obtained with the parameters given in Table 3.

It was found that the dipolar coupling is roughly four times stronger than the exchange coupling and is antiferromagnetic in all cases. This leads to a nonmagnetic exchange ground state, with the first excited (magnetic) level lying ∼1.45 cm^{-1} above the ground. The next closest doublets are nonmagnetic and lie ∼90 cm^{-1} above these. The energies and corresponding tunneling gaps and g_z values of the lowest four exchange doublet states for each molecule are given in Supporting Information, Table S9 and S10. It is found that the splitting of the ground exchange doublet is of the order of 10^{-6} cm^{-1}, indicating that the QTM within each molecule will be relatively weak. This intrinsic tunnelling gap arises because of the non-Kramers nature of the coupled system. Another contribution allowing QTM usually comes from the interaction with transverse magnetic fields induced by the magnetic moments of surrounding complexes; however, since the ground state is nonmagnetic because of antiferromagnetic intracluster exchange, the magnetic field arising from surrounding complexes will diminish with lowering temperature. This is because only the ground (nonmagnetic) state of each molecule remains populated when T approaches 0 K. It is for this reason that we believe the QTM is efficiently suppressed in this unique case.

It is interesting to note the difference in the total exchange between the Gd and Dy analogues, where J = 0 cm^{-1} for **1** but J ≈ −2.93 cm^{-1} for **3**. As recent research of isostructural Ln$_2$ dimers shows,[6c] the Ln−Ln magnetic interactions change monotonically and relatively slowly with the type of lanthanide ion, and since Gd is a close neighbor of Dy, we expect that exchange interactions in the isostructural compounds **1** and **3** should be close in magnitude. The magnetic moments of Gd^{III} and Dy^{III} are roughly 7 μ_B and 10 μ_B (along the main anisotropy axis), respectively, and as the dipolar interaction scales as the square of the magnetic moment, the dipolar contribution for **1** should be roughly half that of **3**. It was
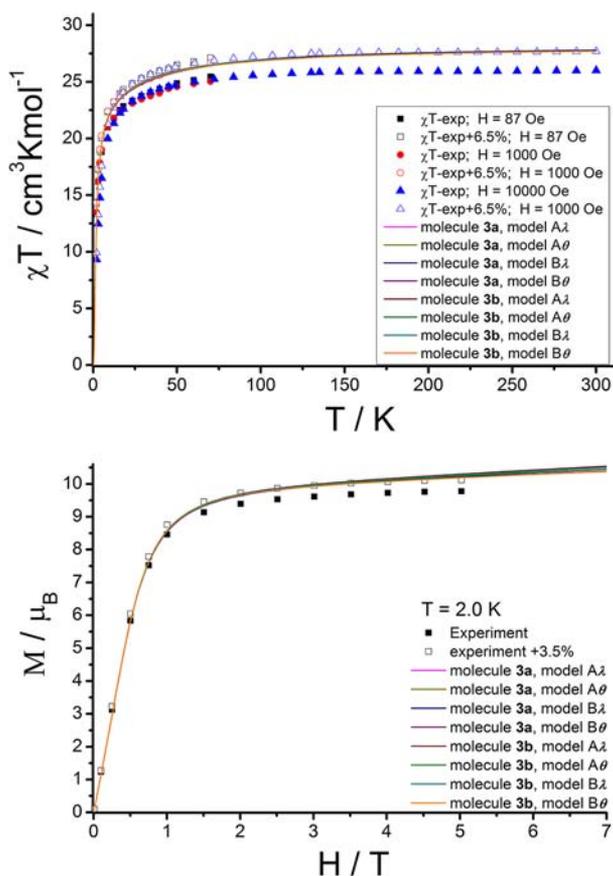
Figure 7. (top) Comparison between the measured and the calculated magnetic susceptibility of **Co₂Dy₂**. An up-scaling of the experimental curve with 6.5% leads to an almost perfect agreement. (bottom) Measured and calculated molar magnetization of **Co₂Dy₂** at 2.0 K. The perfect agreement is achieved if one up-scales the experiment by about 3.5%.

Table 3. Exchange Interactions between the Dy Ions in 3 (cm^{-1})

	model	$J_{dip}{}^a$	J_{exch}	$J_{total} = J_{dip}{}^a + J_{exch}$
molecule 1	Aλ	−2.3018	−0.6195	−2.92128
	Aθ	−2.3989	−0.5363	−2.93519
	Bλ	−2.3001	−0.621	−2.92106
	Bθ	−2.3971	−0.5398	−2.93689
molecule 2	Aλ	−2.4149	−0.5185	−2.93338
	Aθ	−2.4182	−0.539	−2.95717
	Bλ	−2.4169	−0.5205	−2.93735
	Bθ	−2.4197	−0.5393	−2.95893

^{a}Contribution only from the Ising terms $\sim \hat{\tilde{s}}_{1,z}\hat{\tilde{s}}_{2,z}$. In the calculation of the exchange spectrum (Supporting Information, Tables S9 and S10) the dipolar interaction included all terms.

postulated that ZFS on the Gd^{III} ions could mask the presence of the small exchange interaction, as was investigated in ref 6c, where it was shown that reduction of the ZFS on Gd^{III} required a similar reduction of J in the fitting of magnetic data. The possibility of ZFS occurring was investigated by examining the error surface of the calculated vs observed magnetic susceptibility and magnetization for a range of nonzero D and J. Overall there was a sharp minimum around $D \approx 0$ and $J \approx 0$; however, closer inspection revealed two minima within, one at $D = 0.0625$ cm^{-1}, $J = 0.00262$ cm^{-1} and the other at $D =$

−0.0446 cm^{-1}, $J = 0.00228$ cm^{-1}. The magnitude of D is comparable with that calculated[6c] for Gd^{III} where $|D| \sim 0.03$ cm^{-1}. Therefore it seems unlikely that the total coupling interaction is of the same order of magnitude as that for the Dy^{III} case, even with significant ZFS, possibly hinting to a mutual cancellation of the dipolar and exchange components of the interactions. While these two solutions gave numerically better fits to the data, they are visually indistinguishable from the $D = 0$, $J = 0$ fit and definitely within experimental error (measurement and sample). Therefore we cannot confirm or refute the presence of any ZFS or coupling interactions with the powder magnetic data alone, for **1**, and further experiments are required.

Dilution Study of the Dy Analogue in a Y Diamagnetic Matrix. The observed experimental results backed up by ab initio calculations provide us with evidence that complex **3** is a single-molecule magnet and that the QTM is efficiently suppressed at zero-field because of the weak intramolecular antiferromagnetic exchange interactions. The question as to whether compound **3** contains two weakly coupled SIMs, or if the SMM properties arise only from the whole molecule is an intriguing one. One may suggest that at the temperatures studied (exceeding the exchange splitting in the complex) the blocking of the magnetization takes place on individual Dy^{III} ions, so we have effectively two weakly coupled single-ion SMMs (SIMs). One potential way of determining this is the use of magnetic dilution experiments. In a recent article by Habib et al. who performed Squid and micro-Squid measurements on a Dy$_2$ SMM diluted to various ratios in a diamagnetic Y$_2$ matrix, it was concluded that the mechanism in their case was of single ion origin, with the weak intramolecular interactions affecting the relaxation mechanism.[20] To gain further insight on the relaxation process for compound **3** we performed a similar experiment. We first synthesized the diamagnetic {Co^{III}$_2$Y^{III}$_2$} analogue (**4**) to confirm it is isostructural to **3** (See Supporting Information for experimental and X-ray details), and then subsequently isolated the 5% dysprosium diluted compound. This was made up by the addition of Y(NO$_3$)$_3$·6H$_2$O/Dy(NO$_3$)$_3$·6H$_2$O in a 95:5 percentage ratio (See Supporting Information for details). The resulting complex contains three possible products (ignoring the Co^{III} ions), namely, the Y$_2$, YDy, and Dy$_2$ species. The probabilities of observing the different dinuclear species at the 5% dysprosium dilution level are Y$_2$, 90.25%, YDy, 9.5%, and Dy$_2$, 0.25%; therefore, the major paramagnetic product will be the single ion YDy species.[20] AC susceptibility measurements were then performed on a polycrystalline sample of the diluted complex to probe the slow relaxation of the magnetization and the quantum tunneling effects. Under a zero applied DC field and with an oscillating AC field between 0.1–1500 Hz, in the 1.8–18 K temperature range, the data show a marked difference for the diluted sample compared to that found for compound **3** (Figure 8 and Supporting Information, Figure S15).

For the diluted sample the clear frequency-dependent maxima which are present for **3** are now obscured by the presence of a second increase or a peak "tail" below 8 K. These tails at low temperatures are indicative of QTM, which is suppressed for the undiluted complex **3**. Furthermore, the χ'' vs ν plot (Supporting Information, Figure S15) is also markedly different and now only displays temperature independent maxima at the higher frequencies measured, indicating a quantum regime with a fast tunneling time. The blocking of the
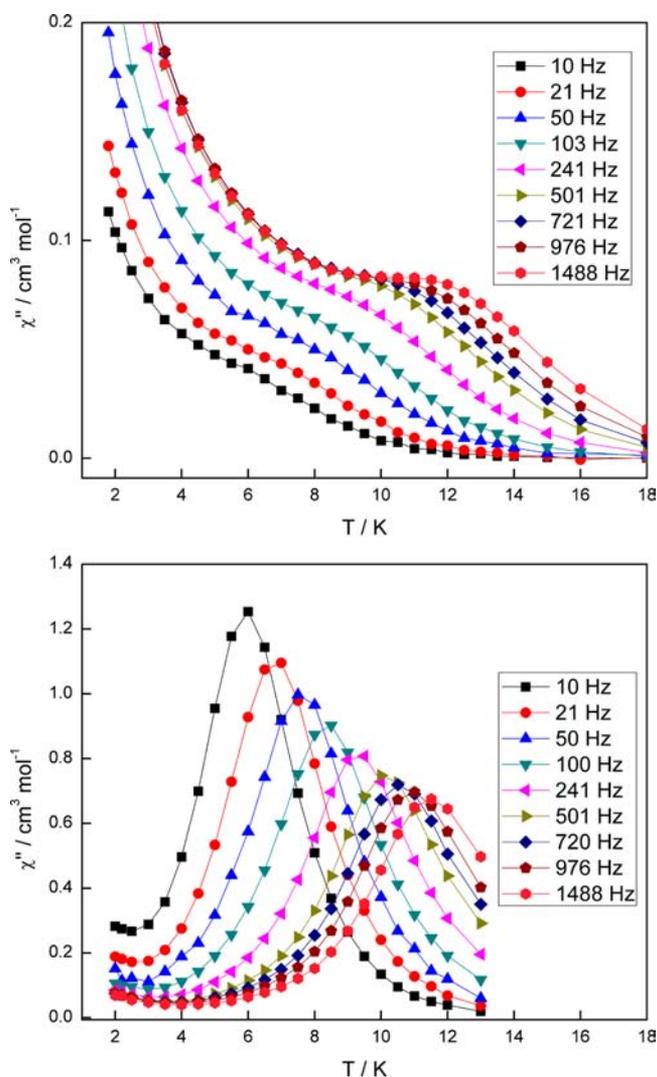
Figure 8. (top) Temperature dependence of the out-of-phase susceptibility (χ'') for the 5% Dy diluted sample; (bottom) Comparison to the temperature dependence of compound **3**.

magnetic moments however appears to occur in a similar temperature region for both diluted and nondiluted samples, indicating that the relaxation barriers in the two systems are similar. This result indicates that the major paramagnetic component in the diluted experiment, the YDy species, is primarily responsible for the slow relaxation mechanism; hence, the relaxation in the case of **3** is of single ion origin. Furthermore the presence of the YDy species reveals that the QTM is now active at zero field, confirming that the weak intramolecular exchange interaction between the Dy ions in **3** suppresses the QTM in this system as predicted by the ab initio calculations. Further micro-Squid experiments using single crystals would be needed to further investigate the relaxation mechanism and QTM in compound **3** and subsequent diluted samples. The results presented here indicate a strategy to develop better performing Dy$_2$ SMMs; the single ion properties should be tuned to achieve ideal slow relaxation behavior, while allowing for a small antiferromagnetic exchange interaction between the metals to suppress the QTM.

■ CONCLUSIONS

In summary, three new heterometallic tetranuclear {d block (Co^{III})–f block (Gd, Tb, Dy)} complexes have been isolated utilizing triethanolamine and benzoic acid as bridging ligands. For the {Dy$^{III}_2$Co$^{III}_2$} analogue, single molecule magnet (SMM) behavior is displayed with a large thermally activated anisotropy barrier of 88.8(2) K. The {Tb$^{III}_2$Co$^{III}_2$} complex showed field-induced SMM behavior. It was also found that the QTM was greatly reduced in the {Dy$^{III}_2$Co$^{III}_2$} example compared to previously reported Dy SMMs because of weak antiferromagnetic dipolar coupling. Together, these features make the {Dy$^{III}_2$Co$^{III}_2$} complex one of the best Dy–Dy SMMs to date. Ab initio calculations have quantified the dipolar and exchange contributions as well as single-ion properties such as g-tensor anisotropy and the direction of the anisotropy axis on each molecule. The calculated, very low value of the tunneling gap in the ground and first excited exchange doublets of Dy$^{III}_2$Co$^{III}_2$ ($\sim$10^{-6} cm^{-1}) explains why the QTM is greatly reduced in this complex. Dilution studies suggest that the relaxation mechanism is of single ion character and that the interaction with the neighboring ion is indeed vital to the suppression of the QTM at zero-field. Current work on related Dy$^{III}_2$Co$^{III}_2$ species involves changing both the coordination environment around the Dy ions, often in a subtle manner, and the crystal packing of such compounds and noting the important changes observed in the dynamic relaxation effects and QTM compared to compound **3**. These results will be reported in due course.

Finally, we note that nonmagnetic doublet states are a fingerprint of polynuclear complexes of strongly anisotropic metal ions, notably lanthanides.[21a] Contrary to the cases of isotropic magnetic complexes, nonmagnetic states can only arise as spin singlets, that is, nondegenerate electronic states. The interest for doublet states arose recently in connection with the design of qubits for quantum computation,[8e,22] which in the case of nonmagnetic doublets, like the antiferromagnetic Ising states in the present Dy$^{III}_2$Co$^{III}_2$ complex (Figure 6) or toroidal magnetic states in Dy$_3$ triangles,[21a,23] or Dy$_6$ hexagons[24] are protected from an external homogeneous magnetic field.[21b] Such states can, in principle, be controlled and manipulated by external electric fields or electronic currents.[21c,d]

■ ASSOCIATED CONTENT

⑤ Supporting Information

Crystallographic data in CIF format; Figures S1–S3, thermal ellipsoid plots; Figures S4 and S5, packing diagrams, Figures S6–S8, DC magnetic data; Figures S9–S13, AC magnetic data; Tables S1–S10 and Figure S14, ab initio calculations; Figure S15, details on yttrium analogue dilution studies including AC magnetic data. This material is available free of charge via the Internet at http://pubs.acs.org.

■ AUTHOR INFORMATION

Corresponding Author
*E-mail: keith.murray@monash.edu (K.S.M.), Liviu. Chibotaru@chem.kuleuven.be (L.F.C.).

Notes
The authors declare no competing financial interest.

■ ACKNOWLEDGMENTS

■ REFERENCES

(1) Sessoli, R.; Powell, A. *Coord. Chem. Rev.* **2009**, *253*, 2328.

(2) (a) Rhinehart, J. D.; Long, J. R. *Chem. Sci.* **2011**, *2*, 2078. (b) Sorace, L.; Benelli, C.; Gatteschi, D. *Chem. Soc. Rev.* **2011**, *40*, 3092.

(3) Ishikawa, N.; Sugita, M.; Ishikawa, T.; Koshihara, S.; Kaizu, Y. *J. Am. Chem. Soc.* **2003**, *125*, 8694.

(4) (a) Lin., P.-H.; Burchell, T. J.; Ungur, L.; Chibotaru, L. F.; Wernsdorfer, W.; Murugesu, M. *Angew. Chem., Int. Ed.* **2009**, *48*, 9489. (b) Blagg, R. J.; Muryn, C. A.; McInnes, E. J. L.; Tuna, F.; Winpenny, R. E. P. *Angew. Chem., Int. Ed.* **2011**, *50*, 6530. (c) Blagg, R. J.; Tuna, F.; McInnes, E. J. L.; Winpenny, R. E. P. *Chem. Commun.* **2011**, *47*, 10587. (d) Hewitt, I. J.; Tang, J.; Madhu, N. T.; Anson, C. E.; Lan, Y.; Luzon, J.; Etienne, M.; Sessoli, S.; Powell, A. K. *Angew. Chem., Int. Ed.* **2010**, *49*, 1.

(5) Milios, C. J.; Vinslava, A.; Wernsdorfer, W.; Moggach, S.; Parsons, S.; Perlepes, S. P.; Christou, G.; Brechin, E. K. *J. Am. Chem. Soc.* **2007**, *129*, 2754.

(6) (a) Layfield, R. A.; McDouall, J. J. W.; Sulway, S. A.; Tuna, F.; Collison, D.; Winpenny, R. E. P. *Chem.—Eur. J.* **2010**, *16*, 4442. (b) Sulway, S. A.; Layfield, R. A.; Tuna, F.; Wernsdorfer, W.; Winpenny, R. E. P. *Chem. Commun.* **2012**, *48*, 1508. (c) Long, J.; Habib, F.; Lin, P.-H.; Korobkov, I.; Enright, G.; Ungur, L.; Wernsdorfer, W.; Chibotaru, L.; Murugesu, M. *J. Am. Chem. Soc.* **2011**, *133*, 5319.

(7) (a) Rhinehart, J. D.; Fang, M.; Evans, W. J.; Long, J. R. *Nat. Chem.* **2011**, *3*, 538. (b) Rhinehart, J. D.; Fang, M.; Evans, W. J.; Long, J. R. *J. Am. Chem. Soc.* **2011**, *133*, 14236.

(8) (a) Leuenberger, M.; Loss, D. *Nature* **2001**, *410*, 789. (b) Bogani, L.; Wernsdorfer, W. *Nat. Mater.* **2008**, *7*, 179. (c) Vincent, R.; Klyatskaya, S.; Ruben, M.; Wernsdorfer, W.; Balestro, F. *Nature* **2012**, *488*, 357. (d) Van Der Zant, H. S. J. *Nat. Nanotechnol.* **2012**, *7*, 555. (e) Wernsdorfer, W. *Nat. Nanotechnol.* **2009**, *4*, 145. (f) Urdampilleta, M.; Klyatskaya, S.; Cleuziou; Ruben, M.; Wernsdorfer, W. *Nat. Mater.* **2011**, *10*, 502.

(9) For example: (a) Rigaux, G.; Inglis, R.; Morrison, S.; Prescimone, A.; Cadiou, C.; Evangelisti, M.; Brechin, E. K. *Dalton Trans.* **2011**, *40*, 4797. (b) Langley, S. K.; Moubaraki, B.; Murray, K. S. *Dalton Trans.* **2010**, *39*, 5066.

(10) (a) Chilton, N. F.; Langley, S. K.; Moubaraki, B.; Murray, K. S. *Chem. Commun.* **2010**, *46*, 7787. (b) Langley, S. K.; Ungur, L.; Chilton, N. F.; Moubaraki, B.; Chibotaru, L. F.; Murray, K. S. *Chem.—Eur. J.* **2011**, *17*, 9209. (c) Langley, S. K.; Chilton, N. F.; Moubaraki, B.; Hooper, T.; Brechin, E. K.; Evangelisti, M.; Murray, K. S. *Chem. Sci.* **2011**, *2*, 1166.

(11) McPhillips, T. M.; McPhillips, S. E.; Chiu, H. J.; Cohen, A. E.; Deacon, A. M.; Ellis, P. J.; Garman, E.; Gonzalez, A.; Sauter, N. K.; Phizackerley, R. P.; Soltis, S. M.; Kuhn, P. *J. Synchrotron Radiat.* **2002**, *9*, 401−406.

(12) Kabsch, W. *J. Appl. Crystallogr.* **1993**, *26*, 795−800.

(13) Sheldrick, G. M. *Acta Crystallogr., Sect. A* **2008**, *A64*, 112.

(14) Casanova, D.; Llunell, M.; Alemany, P.; Alvarez, S. *Chem.—Eur. J.* **2005**, *11*, 1479.

(15) Chilton, N. F. unpublished work.

(16) Gatteschi, D.; Sessoli, R.; Villain, J.; *Molecular Nanomagnets*; Oxford Universiy Press; Oxford, U.K., 2006.

(17) Guo, Y.-N.; Xu, G.-F.; Wernsdorfer, W.; Ungur, L.; Guo, Y.; Tang, J.; Zhang, H.-L.; Chibotaru, L. F.; Powell, A. K. *J. Am. Chem. Soc.* **2011**, *133*, 11948.

(18) For example: (a) Yamashita, A.; Watanabe, A.; Akine, S.; Nabeshima, T.; Nakano, M.; Yamamura, T.; Kajiwara, T. *Angew. Chem., Int. Ed.* **2011**, *50*, 4016. (b) Feltham, H.; Klower, F.; Cameron, S. A.; Larsen, D. S.; Lan, Y.; Tropiano, M.; Faulkner, S.; Powell, A. K.; Brooker, S. *Dalton Trans* **2011**, *40*, 11425.

(19) Lines, M. E. *J. Chem. Phys.* **1971**, *55*, 2977.

(20) Habib, F.; Lin, P.-H.; Long, J.; Korobkov, I.; Wernsdorfer, W.; Murugesu, M. *J. Am. Chem. Soc.* **2011**, *133*, 8830.

(21) (a) Chibotaru, L. F.; Ungur, L.; Soncini, A. *Angew. Chem., Int. Ed.* **2008**, *47*, 4126. (b) Soncini, A.; Chibotaru, L. F. *Phys. Rev. B* **2008**, *77*, 220406. (c) Plokhov, D. I.; Popov, A. I.; Zvezdin, A. K. *Phys. Rev. B* **2011**, *84*, 224436. (d) Soncini, A.; Chibotaru, L. F. *Phys. Rev. B* **2010**, *81*, 132403.

(22) Aromi, G.; Aguila, D.; Gamez, P.; Luis, F.; Roubeau, O. *Chem. Soc. Rev.* **2012**, *41*, 537.

(23) Novitchi, Gh.; Pilet, G.; Ungur, L.; Moshchalkov, V. V.; Wernsdorfer, W.; Chibotaru, L. F.; Luneau, D.; Powell, A. K. *Chem. Sci.* **2012**, *3*, 1169.

(24) (a) Langley, S. K.; Moubaraki, B.; Forsyth, C. M.; Gass, I. A.; Murray, K. S. *Dalton Trans.* **2010**, *39*, 1705. (b) Ungur, L.; Langley, S. K.; Hooper, T. N.; Moubaraki, B.; Brechin, E. K.; Murray, K. S.; Chibotaru, L. F. *J. Am. Chem. Soc.*, Accepted.